Optics Letters

Double-clad ytterbium-doped tapered fiber with circular birefringence as a gain medium for structured light

Iuliia Zalesskaia,[1,*] Yuhao Lei,[2] Peter G. Kazansky,[2] Katrin Wondraczek,[3] Regina Gumenyuk,[1,4] and Valery Filippov[4]

[1] Tampere University, Korkeakoulunkatu 3, Tampere 33720, Finland
[2] Optoelectronics Research Centre, University of Southampton, Southampton, SO17 1BJ, United Kingdom
[3] Dept. Leibniz Institute of Photonic Technology E.V., Albert-Einstein-Str. 9, Jena, 07745, Germany
[4] Ampliconyx Ltd., Lautakatonkatu 18, Tampere 33580, Finland
*iuliia.zalesskaia@tuni.fi

Received 21 September 2023; revised 9 November 2023; accepted 22 November 2023; posted 27 November 2023; published 3 January 2024

Amplifying radially and azimuthally polarized beams is a significant challenge due to the instability of the complex beam shape and polarization in inhomogeneous environment. In this Letter, we demonstrated experimentally an efficient approach to directly amplify cylindrical-vector beams with axially symmetric polarization and doughnut-shaped intensity profile in a picosecond MOPA system based on a double-clad ytterbium-doped tapered fiber. To prevent polarization and beam shape distortion during amplification, for the first time to the best of our knowledge, we proposed using the spun architecture of the tapered fiber. In contrast to an isotropic fiber architecture, a spun configuration possessing nearly circular polarization eigenstates supports stable wavefront propagation. Applying this technique, we amplified the cylindrical-vector beam with 10 ps pulses up to 22 W of the average power at a central wavelength of 1030 nm and a repetition rate of 15 MHz, maintaining both mode and polarization stability.

Published by Optica Publishing Group under the terms of the Creative Commons Attribution 4.0 License. Further distribution of this work must maintain attribution to the author(s) and the published article's title, journal citation, and DOI.

https://doi.org/10.1364/OL.506083

Cylindrical-vector beams with axially symmetric polarization and doughnut-shaped intensity profiles have garnered significant interest in recent decades. This attention is attributed to the broad range of applications, such as high-resolution microscopy [1,2], plasmons excitation [3], particle acceleration [4] and trapping [5,6], optical data storage [7], and high-performance material processing [8,9]. However, building a stable, high-power, short-pulse source with high polarization purity and homogeneous annular mode field distribution by exploiting fiber-based approach presents a challenging task due to high mode instability in symmetrical optical waveguide under an environmental disturbance. The typical approach for generating high power radially and azimuthally polarized beams involves excitation of the beam by a spatially variant wave plate (S-wave plate) or q-plate and then amplification in an isotropic large mode area (LMA) fiber [10,11]. This approach has been implemented for both continuous wave (CW) [10], nanosecond [11], and hundred-picosecond laser systems [12]. However, internal inhomogeneity of the isotropic LMA fiber unavoidably leads to the distortion of the spatial intensity and polarization distribution along the propagation and amplification process, limiting the beam quality performance. This fiber inhomogeneity originates from the number of external and internal perturbations such as bends, transversal compression, elliptical core, and built-in stresses due to variation of dopant distributions [13]. These perturbations are inevitable characteristics of any isotropic fibers becoming even more pronounced in LMA fibers due to a large core area. Recently, we have demonstrated a promising approach for the improvement of LMA fiber homogeneity and the decrease of internal stresses by means of imperfection averaging along the fiber length. This can be done by rapid rotation of the preform during the drawing process resulting in high symmetrization of the core and leading to low internal birefringence. This fiber, the so-called spun-tapered double-clad fibers (sT-DCF) [13,14], features nearly circular polarization Eigenstates maintaining complex beam polarization with minimal distortion. A fiber twist introduces periodic perturbations leading to symmetry violations and formation of a new stable mode structure supporting propagation of optical vortexes or cylindrical-vector modes [15]. Furthermore, spun fibers with twist-induced circular birefringence feature the difference in effective refractive indexes for right and left circular polarizations [16], as well as for even and odd modes and symmetric and antisymmetric modes [17], lifting the mode degeneracy of cylindrical-vector modes. In addition, the tapered longitudinal profile of the LMA fiber is a proven technique for the elevation of thresholds for nonlinear effects and efficient direct amplification of short pulses up to MW-level peak power and several hundred watts of average power with several tens of microjoule pulse energy [18]. Therefore, the combination of spun and taper architectures has great potential to become a versatile technique for delivering high-power short-pulsed signals with complex spatial and polarization profiles.

0146-9592/24/020270-04 Journal © 2024 Optica Publishing Group

Corrected 9 January 2024

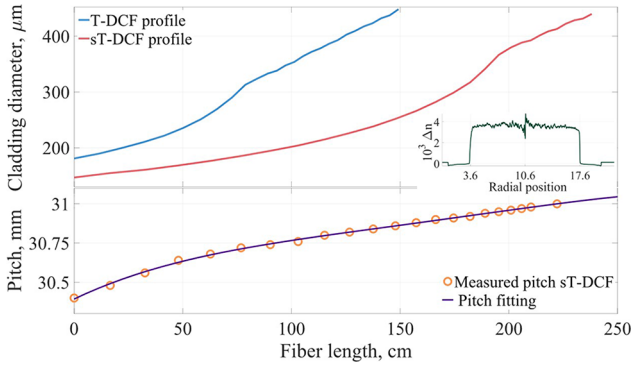

Fig. 1. Top graph: T-DCF and sT-DCF longitudinal profiles. Middle right inset: cross section of the refractive index profile of the initial core material. Bottom graph: pitch variation of the sT-DCF along the length.

In this paper, we demonstrate a successful direct amplification of cylindrical-vector beams carrying short pulses in Yb-doped sT-DCF retaining both beam structure and polarization profiles. The laser system amplifies 10 ps pulses up to 22 W of average power at the central wavelength of 1030 nm at a repetition rate of 15 MHz. We compare the achieved results in the same laser system with the amplification in isotropic Yb-doped tapered double-clad fiber (T-DCF) to confirm the advantage of the spun architecture in maintaining the beam shape and polarization stability.

Both sT-DCF and T-DCF were manufactured by using a step-index Yb-doped preform produced by REPUSIL technology. A cross-sectional refractive index profile of the initial core material is illustrated in Fig. 1 (inset). At a wavelength of 976 nm, the in-core absorption coefficient was measured to be 650 dB/m, while the numerical aperture was determined to be 0.1. The preform was constructed with a core/cladding-diameter ratio (CCDR) equal to 11.5. In order to achieve the desired fiber tapering, a continuous variation of the fiber drawing speed was applied. Additionally, for the sT-DCF, a constant preform rotation velocity was implemented during the drawing process to impart the spun architecture. The fibers underwent a tapering process wherein the outer cladding diameter was gradually reduced along a 7 m length, resulting in a final cladding diameter range of 90 μm to 500 μm. To ensure the undistorted propagation of the TM_{01} mode, the T-DCF was cut to core/cladding diameters ranging from 16/185 μm to 40/460 μm, while the sT-DCF was cut to a core/cladding diameter ranging from 12.7/146 μm to 37.5/431 μm. The cladding diameter fiber profiles are shown in the top graph in Fig. 1. A V number of the thin side was equal to 5.04 at 1030 nm for T-DCF and 4 for sT-DCF.

Due to the variation in the drawing speed during the tapering process, the pitch of the sT-DCF slightly changed along the length of the fiber in conjunction with the diameter reduction. The measured pitch sT-DCF profile is presented in Fig. 1 (bottom graph). The pitch value of sT-DCF slightly increased from 30.4 mm at the thinnest side to 31 mm when the sT-DCF core diameter reached 37.5 μm.

In the experimental configuration, a linearly polarized beam carrying 10 ps pulses at a 15 MHz repetition frequency was generated by a seed laser mode-locked with a nonlinear amplifying loop mirror (NALM) as depicted in Fig. 2.

These pulses were subsequently guided into the Yb-doped fiber pre-amplifier, after which they were ultimately yielding an average output power of 50 mW. This stage includes an approximately 160 cm long segment of polarization-maintaining (PM), Panda-type ytterbium-doped fiber (YDF) (Coherent PM-YSF-HI-HP) with a core diameter of 6 μm and a cladding diameter of 125 μm. A 976 nm single-mode laser diode supplied 250 mW pump power was used for pumping the PM-YDF, effectively amplifying the pulses. The resulting beam was then directed toward an S-wave plate, where a radially polarized beam was formed. With a diameter of 5 mm, the S-wave plate was imprinted using birefringence patterning on an infrared-grade synthetic silica glass substrate with an ultrafast laser, operating at 1030 nm with a pulse duration of 600 fs. The wave plate's retardance was tailored to half of the 1050 nm wavelength, and its slow axis azimuth was set at half the polar angle. Writing parameters, including the pulse energy, scan speed, and a focusing objective NA of 0.16, were optimized to produce a birefringent X-type modification with a characteristic feature of randomly distributed anisotropic nanopores in silica glass. This specific type of birefringence is characterized by its excep-

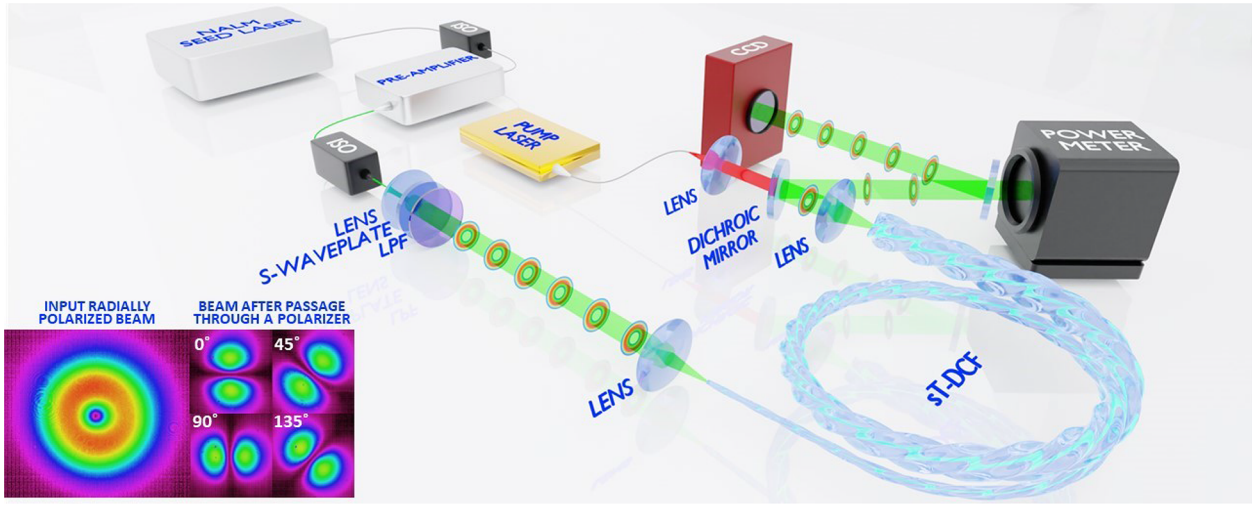

Fig. 2. Schematic of the experimental setup, ISO, optical isolator; CCD, charged coupled device; LPF, long-pass filter. Inset: converted by S-wave plate radially polarized beam (left); radially polarized beam after passage through a rotated linear polarizer at four polarizer axis positions (0°, 45°, 90°, and 135°) (right).

tionally high transmission [19]. The measured transmission of the fabricated S-wave plate exceeded 99% with reference to an untreated silica glass sample at a wavelength of 1050 nm and the damage threshold was about 1.56 J/cm^2 for a 1030 nm, 300 fs laser beam [20], which is close to pristine silica glass. The transformed radially polarized beam exhibited a prominent doughnut-shaped intensity profile in the far field, as depicted in the inset in Fig. 2.

The beam quality parameter M^2 for the converted beam was nearly 2.11, which closely corresponds to the theoretical value of 2 for radially polarized beams. The beam was guided through a rotated linear polarizer featuring a two-lobed intensity profile for 0°, 45°, 90°, and 135°polarizer axis [Fig. 2 (inset)] indicating that the resultant vector beam maintains high polarization distribution uniformity. To safeguard the pre-amplifier from potential damage due to the backward pump of the tapered fiber, a long-pass filter was integrated into the setup. Finally, the radially polarized beam was injected into the high-power amplifier. In the first experiment, we employed a T-DCF as our amplification medium. The primary amplifier stage consisted of a T-DCF with a length of approximately 2.5 m. The thin input side of the T-DCF featured a core diameter of 16 μm and a numerical aperture (NA) of 0.1, while the opposing side had a larger core diameter of about 40 μm. With an input V-number of 5.04 at 1030 nm, the T-DCF is capable of supporting the propagation of the TM_{01} mode. To avoid any excess propagation loss, the T-DCF was loosely coiled with a large bend diameter of around 30 cm. The thinner side of T-DCF was perpendicularly cleaved in order to achieve the highest efficiency of radially polarized beam injection without any distortion. Meanwhile, the output end facet was angle-cleaved at an angle of approximately 4textdegree to prevent backreflection. The T-DCF was counter-pumped using a fiber-coupled 976 nm high-power wavelength-stabilized diode laser (BWT K976AG1RN), pigtailed with a 105 μm core diameter fiber and a numerical aperture of 0.22. In this configuration, the final stage of the amplifier reached an optical-to-optical efficiency of 46% from the total pump power to the T-DCF output power, yielding an output power of 30 W measured directly at the fiber output. We conducted an extensive analysis of the beam quality under varying pump power levels. For a relatively low-pump power of 5 W, which generated an output power of 0.11 W, the measured beam quality was 2.17. When the pump power was increased to 65 W, resulting in an output power of 30 W the beam quality slightly rose to 2.21. The output beam intensity profiles and spectrums corresponding to these measurements can be found in Fig. 3.

Upon closely examining the beam intensity profile images, it appears that the beams display some degree of distortion. To provide further evidence for this observation, we measured the azimuthal-intensity profile for radius r after beam passage through a linear polarizer. The normalized distribution of these measurements is illustrated in Fig. 4 (center).

To further investigate the polarization properties of the output beams, we introduced a polarizer to the output beam path for both the slightly pumped propagated beam and the highly pumped one. As the intensity profile of the 30 W beam passed through a rotating linear polarizer (depicted in Fig. 4), for four polarizer axes (0°, 45°, 90°, and 135°), it did not exhibit a pure two-lobe form. This observation suggests that the resulting vector beam may possess a relatively low polarization distribution uniformity.

In the second experiment, an sT-DCF was investigated as an alternative to the T-DCF utilized in the first experiment, with

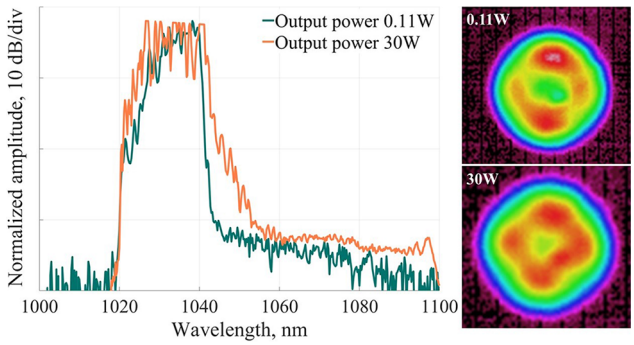

Fig. 3. Experimental T-DCF output spectrums for 0.11 W and 30 W output power (left). Experimental output intensity distributions in the near-field for 0.11 W (top right) and 30 W (bottom right) output power.

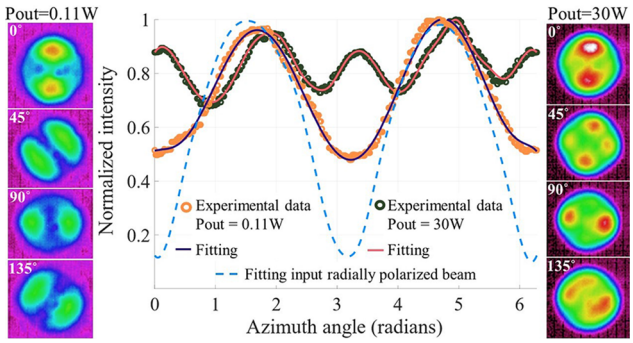

Fig. 4. About 0.11 W output T-DCF beam after passage through a rotated linear polarizer for four polarizer axis 0°, 45°, 90°, and 135°(left). Normalized azimuthal-intensity profile for radius r after T-DCF beam passage through a linear polarizer (center). 30 W output sT-DCF beam after passage through a rotated linear polarizer for four polarizer axes 0°, 45°, 90°, and 135°(right).

core diameters ranging from 12.7 μm to 37.5 μm. This configuration, possessing a V-number of 4 from the thin side of the fiber, facilitated the propagation of the radially polarized TM_{01} mode within the core. The output beam was examined at various pump power levels. We indicated that with a 5 W pump power, the output power reached 0.34 W, and the beam quality was measured at 1.98. As the pump power increased to 52 W, the output power reached the level of 22.07 W, corresponding to a 42% optical-to-optical efficiency, and the beam quality experienced a slight improvement to 1.96. The cause for the beam quality being below the theoretical limit of 2 can be elucidated by the dominance of the LP_{11} mode on the x axis at elevated power levels [10]. The output beam intensity profiles and spectrums corresponding to these power levels are depicted in Fig. 5.

To thoroughly investigate the polarization state, as in the first experiment, a rotating linear polarizer was employed. The intensity profiles of the beam after passing through the rotating linear polarizer at four polarizer axis positions (0°, 45°, 90°, and 135°) for both high- and low-pump power levels are presented in Fig. 6, showcasing the preservation of the complex polarization profile.

Additionally, the normalized azimuthal-intensity profile for radius r after passage through a linear polarizer is depicted in Fig. 6, further corroborating the preservation of the complex polarization profile. The exceptional preservation of polarization in the sT-DCF can be attributed to its spun architecture,

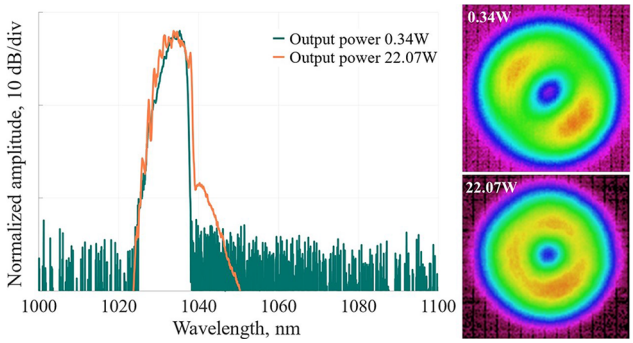

Fig. 5. Experimental sT-DCF output spectrums for 0.34 W and 22.07 W output power (left). Experimental output intensity distributions in the near field for 0.34 W (top right) and 22.07 W (bottom right) output power.

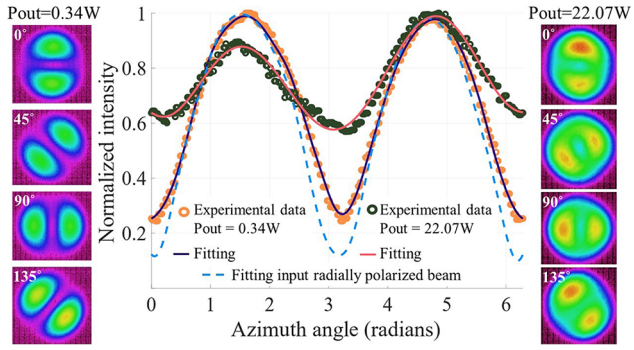

Fig. 6. About 0.34 W output sT-DCF beam after passage through a rotated linear polarizer for four polarizer axis 0°, 45°, 90°, and 135°(left). Normalized azimuthal-intensity profile for radius r after sT-DCF beam passage through a linear polarizer (center). 22.07 W output sT-DCF beam after passage through a rotated linear polarizer for four polarizer axes 0°, 45°, 90°, and 135°(right).

which leads to an upper isotropic nature and, subsequently, low birefringence.

In both experiments with T-DCF and sT-DCF, the M^2 factor remains stable over a range of pump and output power levels. Figure 7 presents a comparative variation of the M^2 factor relative to the output power.

In conclusion, we demonstrated the robust solution for the amplification of cylindrical-vector beams with axially symmetric polarization and a doughnut-shaped intensity profile. The active spun double-clad tapered fiber maintained high modal purity during the amplification process due to its special transverse and longitudinal architecture. The radially polarized beam carrying 10 ps at 10 MHz repetition rate was successfully amplified up to 22 W at 1030 nm retaining both spectral and polarization profiles. The future work will be focused on the optimization of the geometrical architecture of sT-DCF to improve

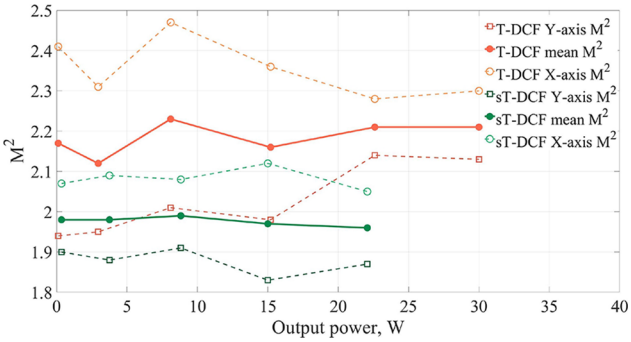

Fig. 7. M^2 factor variation relative to output power for T-DCF and sT-DCF.

the amplification process and demonstrate further power scaling maintaining mode parameters.

Funding. HORIZON EUROPE European Innovation Council (10109 6317); Academy of Finland (320165); European Research Council (789116).

Acknowledgment. I. Zalesskaia thanks the TLTO doctoral school for the financial support of her Ph.D. study.

Disclosures. The authors declare no conflicts of interest.

Data availability. Data underlying the results presented in this paper are not publicly available at this time but may be obtained from the authors upon reasonable request.

REFERENCES

1. P. Meng, S. Pereira, and P. Urbach, Opt. Express **26**, 29600 (2018).
2. Y. Kozawa, D. Matsunaga, and S. Sato, Optica **5**, 86 (2018).
3. Y. Dong, S. Xi, B. Zhu, *et al.*, Opt. Commun. **443**, 197 (2019).
4. C. Varin, S. Payeur, V. Marceau, *et al.*, Appl. Sci. **3**, 70 (2013).
5. Q. Zhan, Opt. Express **12**, 3377 (2004).
6. K. Dholakia and T. Cižmár, Nat. Photonics **5**, 335 (2011).
7. Y. Zhang and J. Bai, Opt. Express **17**, 3698 (2009).
8. M. Meier, V. Romano, and T. Feurer, Appl. Phys. A **86**, 329 (2007).
9. O. J. Allegre, W. Perrie, S. P. Edwardson, *et al.*, J. Opt. **14**, 085601 (2012).
10. D. Lin, J. M. O. Daniel, M. Gecevičius, *et al.*, Opt. Lett. **39**, 5359 (2014).
11. D. Lin, N. Baktash, M. Berendt, *et al.*, Opt. Lett. **42**, 1740 (2017).
12. D. lin, N. Baktash, S.-U. Alam, *et al.*, Opt. Lett. **43**, 4957 (2018).
13. A. Fedotov, V. Ustimchik, J. Rissanen, *et al.*, Opt. Express **29**, 16506 (2021).
14. A. Fedotov, V. Ustimchik, J. Rissanen, *et al.*, J. Opt. Soc. Am. B **38**, F161 (2021).
15. K. N. Alekseyev and M. A. Yavorsky, Opt. Spectrosc. **102**, 754 (2007).
16. R. Ulrich and A. Simon, Appl. Opt. **18**, 2241 (1979).
17. M. Ornigotti, G. D. Valle, D. Gatti, *et al.*, Phys. Rev. A **76**, 023833 (2007).
18. A. Petrov, M. Odnoblyudov, R. Gumenyuk, *et al.*, Sci. Rep. **10**, 17781 (2020).
19. M. Sakakura, Y. Lei, L. Wang, *et al.*, Light: Sci. Appl. **9**, 15 (2020).
20. G. Shayeganrad, X. Chang, H. Wang, *et al.*, Opt. Express **30**, 41002 (2022).